ACS APPLIED MATERIALS & INTERFACES

Research Article

www.acsami.org

Fabrication of Three-Dimensional (3D) Raspberry-Like Copper Chromite Spinel Catalyst in a Facile Hydrothermal Route and Its Activity in Selective Hydroxylation of Benzene to Phenol

Shankha S. Acharyya, Shilpi Ghosh, and Rajaram Bal*

Catalytic Conversion & Processes Division, CSIR-Indian Institute of Petroleum, Dehradun-248005, India

Supporting Information

ABSTRACT: Three-dimensional (3D) raspberry-like $CuCr_2O_4$ spinel nanoparticles were prepared hydrothermally in the presence of cationic surfactant, cetyltrimethylammonium bromide (CTAB). Detailed characterization of the material was carried out by X-ray diffraction (XRD), inductively coupled plasma−atomic emission spectroscopy (ICP-AES), X-ray photoelectron spectroscopy (XPS), scanning electron microscopy (SEM), transmission electron microscopy (TEM), Fourier transform infrared (FTIR) spectroscopy, and thermogravimetric analysis (TGA). XRD revealed the formation of $CuCr_2O_4$ spinel phase, and SEM showed the formation of a 3D raspberry-like structure, composed of 20−50 nm nanoparticles. The raspberry-like particles exhibited excellent catalytic behavior for the hydroxylation of benzene to phenol with H_2O_2. The influence of reaction parameters were investigated in detail. A benzene conversion of 68.5% with 95% phenol selectivity was achieved at 80 °C. The catalyst did not show any leaching up to 10 reuses, showing the true heterogeneity of the catalyst. However, significant H_2O_2 decomposition occurs on the catalyst necessitating its use in 5-fold excess.

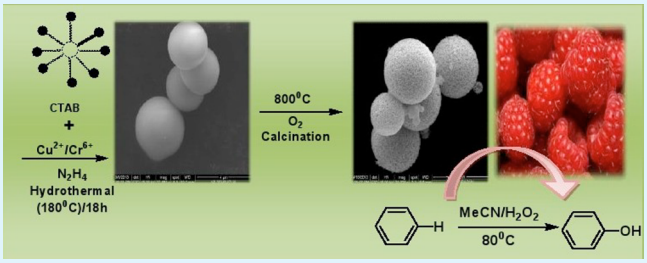

KEYWORDS: *$CuCr_2O_4$ spinel, 3D raspberry, benzene, selective oxidation, phenol*

INTRODUCTION

Three-dimensional (3D) nanostructures have drawn much attention, because of their potential applications, such as catalysis, removal of pollutants in water treatment, use in supercapacitors, etc.[1−6] However, the controlled controlled construction of 3D architectures from nanobuilding blocks via chemical routes still remains a challenge in material chemistry research, because control of the nucleation and growth of nanomaterials is really a mammoth task.[6] The simplest synthetic route to 3D nanostructures is the self-assembly, in which ordered aggregates are formed in a spontaneous process and thus the process has become an important technique to execute fabrication of sophisticated architectures.[6,7] However, the development of simple and reliable synthetic methods for hierarchically self-assembled architectures with designed chemical components and tunable morphologies still remains a challenge for the researchers. Since the first successful preparation of nonporous monodispersed silica spheres by Stober et al.,[8] spheres and spheres on sphere (SOS) have been among the most investigated morphologies, because of their broad applications in areas of catalysis, controlled drug release, and separation science. Fabrication of self-assembled architectures produced from a series of building blocks with a raspberry-like morphology has been projected as one of the intense fields of research.[9] There have been reports on nanomaterials possessing raspberry-like morphologies, such as silica particles,[9,10] gold microspheres,[11] cobalt-hierarchical microspheres,[12] and Fe_3O_4@SiO_2 particles.[13] Xu et al. has reported raspberry-like phenol formaldehyde resin (PFR), where Ag and Au were used to prepare Ag@PFR and Au@PFR colloidosomes with high yields.[14] Recently, Lin and his group reported one-step solvothermal-processed 3D spinel-type manganese dioxide microspheres with a raspberry-like morphology.[5] Composite oxides of Cu and Cr have long been recognized as versatile functional materials, because of their wide commercial applications as a catalyst for various chemical reactions.[15−18] Moreover, its major application lies as a burn rate modifier in solid propellant processing for space launch vehicles.[19−21] Among these oxides, Cu−Cr spinels are considered to be the most effective, because of the tetragonally distorted normal spinel structure, where the more-active Cu^{2+} possesses tetrahedral coordination.[18,19] During the past few decades, considerable attention has been paid in the preparation of Cu−Cr catalysts,[15−17,19−24] but preparation of the surfactant-assisted 3D ordered raspberry-like microspheres of $CuCr_2O_4$ spinel has not been reported to date. Herein, for the first time, we report here the surfactant-assisted preparation of 3D raspberry-like $CuCr_2O_4$ spinel nanoparticles via a hydrothermal synthesis method.

Received: June 13, 2014
Accepted: August 1, 2014
Published: August 1, 2014

Phenol is one of the most important chemical intermediate and its current worldwide production exceeds 10 megaton per annum.[25] Industrially, it is being produced by a cumene process.[26] Apart from being multistep in nature, this process suffers from low yield (~5% based on the amount of benzene initially used) and produces explosive intermediate, cumene hydroperoxide, and unwanted byproducts. Although there have been several reports using different oxidizing agents, such as N_2O,[27] H_2O_2,[28−30] $NH_3 + O_2$,[26,31] air + CO,[32] etc., in most of the cases, the phenol yield is very low. Although researchers have tried the direct hydroxylation of benzene to phenol in the gas phase, the catalyst suffers rapid deactivation due to coke deposition.[33] The use of H_2O_2 as an oxidant in the liquid-phase hydroxylation of benzene is very advantageous, from both environmental and industrial viewpoints;[34] however, in most of the cases, overoxidation of the phenol occurs, forming products such as catechol, resorcinol, or benzoquinone.[25,35] Pinnaivia and his group reported a benzene conversion of 31% with 95% phenol selectivity using titanosilicate (TS-1) catalyst.[36] Vanadium(IV)-based catalysts have been proved to be a promising candidate for activating the C_{sp2}−H bond. A benzene conversion of 34.5% and 100% selectivity toward phenol was reported over a homogeneous catalyst (Keggin-type molydovanadophosphoric acid catalyst in liquid phase).[37] Borah et al. reported the oxidation of benzene to phenol using vanadyl(IV) acetylacetonate grafted to periodic mesoporous organosilica catalyst and H_2O_2 as oxidant to get a benzene conversion of 27% with 100% selectivity.[38] Zhao and his group reported a phenol yield of ~24% using heteropolyanion-paired cross-linked ionic-copolymer [prepared by the anion-exchange of heteropolyacid $H_5PMo_{10}V_2O_{40}$ with poly(divinylbenzene-3-*n*-butyl-1-vinylimidazolium)Br] at 55 °C[39] and thereafter reported a phenol yield of 31% using the nitrile-functionalized POM salt $[C_3CNpy]_4HPMoV_2$, which is a phase-transfer catalyst with H_2O_2 as the oxidant at 60 °C.[40] Recently, Long et al. reported a phenol yield of 14% using C_3N_4−$H_5PMo_{10}V_2O_{40}$ in reductant-free aerobic oxidation of benzene.[41] However, the hydroxylation of benzene in liquid phase is concerned with several issues like either low phenol yield, recyclability of the catalyst and separation of products. Very recently, our group reported 72.5% benzene conversion with a phenol selectivity of 94% over $CuCr_2O_4$ spinel nanoparticles with H_2O_2 as the oxidant.[42] We observed that the activity of the catalystis gradually reduced after the sixth run because of the leaching of Cu(II) from the spinel framework. Therefore, we were in need of a highly stable catalyst that would be recycled several times (at least 10 times) without significant losses in activity. We envisioned that, if a chromium-(VI) precursor is used in the preparation of $CuCr_2O_4$ spinel, a 3D structure of $CuCr_2O_4$ spinel is generated, where the catalyst showed to be devoid of leaching properties apart from displaying high activity in benzene hydroxylation reaction.

Herein, we report the selective oxidation of benzene to phenol using H_2O_2 as oxidant where a benzene conversion of 68.5% with 95% phenol selectivity was achieved at 80 °C over nanocrystallite of $CuCr_2O_4$ spinel catalyst with the unique raspberry-like 3D structure.

EXPERIMENTAL SECTION

Materials and Methods. Ammonium dichromate, copper nitrate, cetyltrimethylammonium bromide (CTAB, 99%), hydrazine monohydrate solution, benzene, acetonitrile, and H_2O_2 (50%) were purchased from Sigma−Aldrich. NH_3 solution was acquired from Acros Organics (for analysis) and doubly distilled water (HPLC grade) was used in the synthesis.

Catalyst Preparation. The 3D $CuCr_2O_4$ spinel nanoparticles catalyst with a raspberry structure was prepared by modifying our own preparation method.[43] The typical preparation method is as follows. An aqueous solution of 2.6 g of $Cu(NO_3)_2{\cdot}3H_2O$ was added with vigorous stirring to 2.7 g of $(NH_4)_2Cr_2O_7$ dissolved in 40 g of deionized water to form a homogeneous solution. The pH of the medium was made to be 9 by adding ammonia solution dropwise. An aqueous solution of 3.2 g of the cationic surfactant cetyltrimethylammonium bromide (CTAB) was added to the Cu−Cr solution mixture. Finally, an aqueous solution of 1.0 g of hydrazine was added dropwise. The reagents were added by maintaining a $CuO:Cr_2O_3$ molar ratio of 1:1 and a Cu:Cr:CTAB:-H_2O:hydrazine ratio of 1:2:0.8:200:1.5. After stirring until a homogeneous solution was obtained, the resultant gel was transferred into Teflon-lined stainless steel autoclave vessel and treated hydrothermally at 180 °C for 18 h under autogenous pressure; after 18 h, the autoclave was cooled to room temperature and the final greenish product was washed with distilled water, acetone, and ethanol and dried at 100 °C, for 10 h under vacuum, followed by calcination at 800 °C for 6 h in air.

We also prepared surfactant promoted copper(II) oxide and chromium(III) oxide in hydrothermal method in the same process to compare their catalytic activities with the prepared $CuCr_2O_4$ raspberry catalyst in a benzene hydroxylation reaction.

CHARACTERIZATION TECHNIQUES

Powder X-ray diffraction (XRD) spectra were collected on a Bruker D8 Avance X-ray diffractometer fitted with a Lynx eye high-speed strip detector and a Cu Kα radiation source. Diffraction patterns in the 2°−80° region were recorded at a rate of 0.5° (2θ) per minute. Scanning electron microscopy (SEM) images were taken on a FEI Quanta 200 F system, using a tungsten filament doped with lanthanum hexaboride (LaB_6) as an X-ray source, fitted with an ETD detector with high vacuum mode using secondary electrons and an acceleration tension of 10 or 30 kV. Samples were analyzed by spreading them on a carbon tape. Energy-dispersive X-ray spectroscopy (EDX) was used in association with SEM for the elemental analysis. The elemental mapping was also collected with the same spectrophotometer. Transmission electron microscopy (TEM) images were collected using a JEOL JEM 2100 microscope, and samples were prepared by mounting an ethanol-dispersed sample on a lacey carbon Formvar-coated copper grid. X-ray photoelectron spectroscopy (XPS) spectra were recorded on a Thermo Scientific K-Alpha XPS spectrometer, and binding energies (±0.1 eV) were determined, with respect to the position of the C 1s peak at 284.8 eV. Chemical analyses of the metallic constituents were performed using inductively coupled plasma−atomic emission spectrometry (ICP-AES) (Model PS 3000 uv, (DRE), Leeman Laboratories, Inc., USA). Thermogravimetric analyses (TGA) of the uncalcined catalyst were carried out in a Pyris Diamond (Perkin−Elmer) and Technology by SII (Seiko Instruments Inc., USA) instrument balance by heating 2.15 mg samples at 5 °C min^{-1} in flowing air. Fourier transform infrared (FT-IR) spectra were recorded on a Thermo Nicolet Model 8700 (USA) instrument with the following operating conditions: resolution, 4 cm^{-1}; number of scans, 36; operating temperature, 23−25 °C; and frequency range, 4000−400 cm^{-1}.

CATALYTIC OXIDATION

Catalytic liquid-phase hydroxylation of benzene was carried out using a two-neck 25-mL round-bottom flask (immersed in a water bath) fitted with a condenser, thermometer, and a magnetic stirrer. In a typical oxidation experiment, 10 mL of

acetonitrile, 1 g of benzene, and 0.08 g of $CuCr_2O_4$ raspberry spinel catalyst were taken in the flask and the reaction temperature was increased to 80 °C. Then, H_2O_2 (50% aqueous solution) was added dropwise, and the resulting mixture was refluxed for the required time. Small aliquots of the sample were withdrawn from the reaction mixture at regular intervals for analysis using a syringe. At the end of the reaction, the solid particles (catalyst) were separated by filtration, and the products were analyzed using a gas chromatography (GC) (Agilent, Model 7890) system equipped with a flame ionization detector (FID) and a HP5 capillary column (30 m length, 0.28 mm id, 0.25 μm film thickness), using methanol as an internal standard. The product identification was carried out by injecting the reference samples and performing GC-MS analyses. The benzene conversion and phenol formation were calculated using a calibration curve (obtained by manual injecting the reference compounds). The individual yields were calculated and normalized with respect to the GC response factors. For the reusability test, the catalyst was repeatedly washed with acetonitrile and acetone and dried overnight at 100 °C and used as such, without regeneration.

RESULTS AND DISCUSSION

Catalyst Characterization. The powder XRD patterns of the Cu−Cr catalysts are shown in Figure 1. The powder XRD

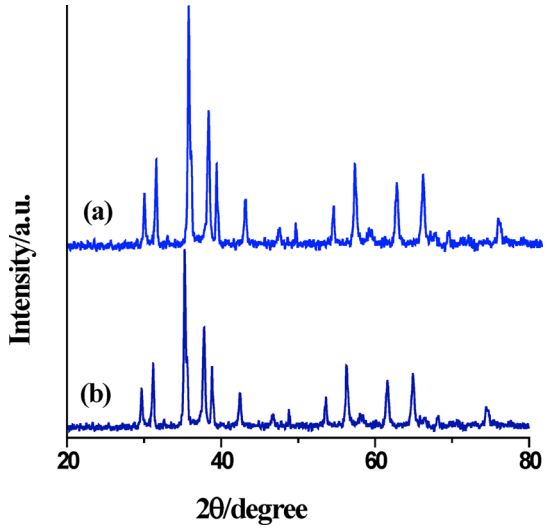

Figure 1. XRD patterns of the three-dimensional (3D) raspberry-like $CuCr_2O_4$ spinel catalyst (a) before and (b) after catalysis (after 10 recycles).

pattern exhibited the typical diffraction lines of the bulk $CuCr_2O_4$ spinel exclusively with the maximum intensity peak at 2θ value of 35.16° (JCPDS File Card No. 05-0657), along with the presence of chromium oxide, as suggested by the peak observed at 40.06° (JCPDS File Card No. 38-1479). The crystallite size was determined using the Scherrer equation (based on 2θ = 35.15°) and a mean particle size of 38.5 nm was observed. A panoramic SEM image (Figure 2) revealed the production of the uniform 3D raspberry-like structures with diameters in the range of 2−5 μm. The yield of product with a 3D raspberry-like morphology is ∼100%. SEM also revealed that the entire raspberry architecture is composed of several nanoparticles in the range of 30−50 nm. Ensembles of these nanoparticles assemble together to form 3D raspberry-like structures. The microspheres continued to grow

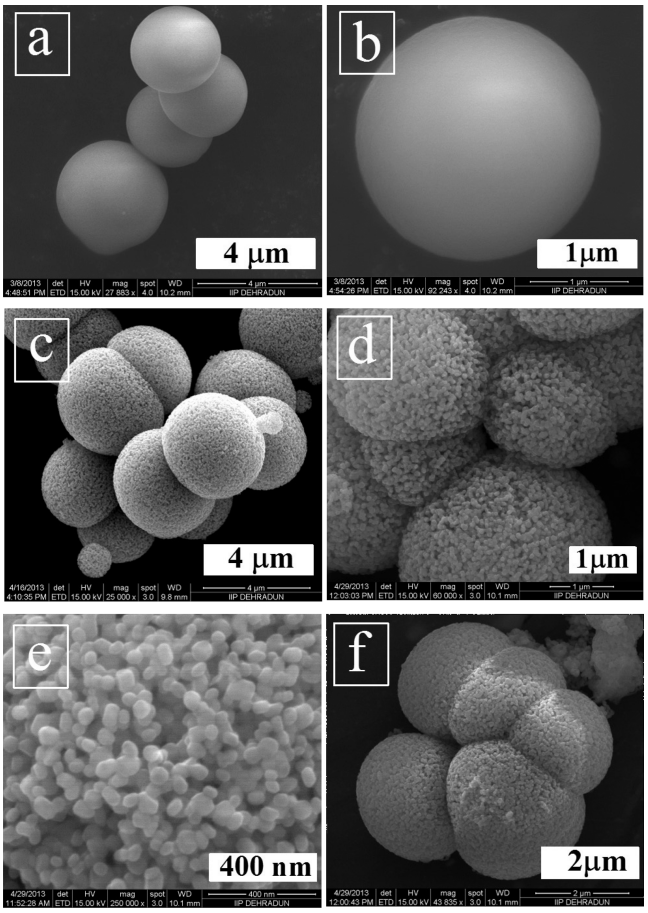

Figure 2. SEM images of (a, b) uncalcined and (c−e) calcined $CuCr_2O_4$ raspberry-like fresh and (f) spent catalyst (after 10 recycles).

by combining with the existing primary particles during hydrothermal treatment and finally form the raspberry-like structure. The surface of the individual particle in the raspberry was smooth (as confirmed by TEM analyses), indicating the good coverage and protection effect of CTAB template during the nucleation and growth of the crystallite. Calcination did not change the overall morphology of the as-synthesized sample (see Figures 2a and 2b, and Table 1). The embedment of the CTA molecules over the precalcined catalyst was confirmed by the FTIR analysis (see Figure 3). The peaks of the sample at 812 and 1062 cm^{-1} can be assigned to the C−N^+ stretching modes of CTAB molecules.[44] The peaks at 1378 and 1462 cm^{-1} are assigned to the symmetric mode of vibration of the head groups of the methylene moiety (N^+−CH_3) and the CH_2 scissoring mode, respectively.[44] The frequencies above 1600 cm^{-1} to 3000 cm^{-1} are due to CH_2 symmetric and antisymmetric vibrations, respectively. Note that the shift of vibrations to lower frequency occurred as the alkyl chains experienced a more hydrophobic environment in Cu−Cr blocks upon the surface of which the CTA moieties were supposed to be bound.[44] It can be inferred that the mutual interactions between CTAB and the Cu−Cr surface have taken place. These typical frequencies were absent when the material was calcined at 800 °C in air (fresh catalyst) in the case of the prepared catalyst, which indicated that the embedded CTAB moieties have been completely removed from the catalyst surface during calcination. The calcined sample also exhibited absorption bands at 608 and 517 cm^{-1}, which refer to the $Cr_2O_4^{2-}$ group in spinel.[6] The absorption bands at 517 cm^{-1}

dx.doi.org/10.1021/am503722t | ACS Appl. Mater. Interfaces 2014, 6, 14451−14459

Table 1. Physicochemical Properties of the $CuCr_2O_4$ Raspberry Spinel Nanoparticles Catalyst

entry	catalyst	BET surface area (m^2/g)	Cu/Cr molar ratio[a]	Particle Size (nm) XRD[b]	Particle Size (nm) TEM	morphology (from SEM)
1	$CuCr_2O_4$ (fresh)	68	0.5	38.5	40	raspberry-like spherical (composed of innumerable nanoparticles)
2	$CuCr_2O_4$ (spent, after 10 recycles)	65	0.5	39.8	40	raspberry-like spherical (composed of innumerable nanoparticles)

[a]Estimated by ICP-AES. [b]Measured using the Scherrer equation.

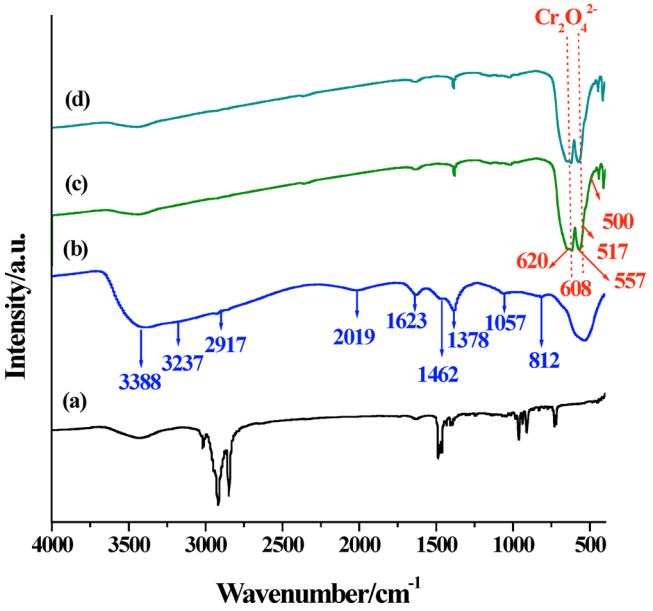

Figure 3. FTIR spectra of pure CTAB (spectrum a), uncalcined (spectrum b), calcined (spectrum c), and spent (after 10 recycles) $CuCr_2O_4$ spinel catalyst (spectrum d).

may also correspond to the stretching vibrations of the Cr−O−Cu. The FTIR spectrum of $CuCr_2O_4$ (Figure 3c) reveals well-resolved absorption bands at 620 cm^{-1}, corresponding to the stretching vibrations of the Cr−O bonds of $CuCr_2O_4$. The band at 517 cm^{-1} is also marked with asymmetric line broadening, indicating the presence of a band at 500 cm^{-1}, which is the characteristic band of Cu−O. The band located at 557 cm^{-1} is the characteristic band of Cr−O.[45] Moreover, it was also confirmed from the FTIR diagram that, there was no structural deformation in the catalyst, even after 10 recycles. Furthermore, in the SEM-EDAX diagram of the fresh catalyst (see Figure S1 in the Supporting Information) does not show any peaks for C, N or even Br, which further confirms the removal of the template (CTAB) by calcination. The embedding of CTAB molecules on the precalcined catalyst surface was further confirmed from TGA analysis. When TGA analysis of the uncalcined sample was performed, in the temperature range of 100°−500 °C, an overall weight loss of 32.6% was observed (see Figure S3 in the Supporting Information), which also supports the presence of CTA moiety in the as-synthesized catalysts. However, transmission electron microscopy (TEM) images at low magnification (Figure 4a) revealed that each unit of the raspberry-like structure was composed of interconnected nanoparticles with smooth surfaces (see the inset of Figure 4a). A representative high-resolution TEM image is shown in Figure 4d. The lattice fringes with a *d*-spacing of 0.30 nm, corresponding to the spacing of the (220) plane of $CuCr_2O_4$ can also be seen.[18] The (220) plane probably regulates the activity and chemical selectivity of the catalyst. Particle size distribution (histogram) based in Figure 4a (TEM image of fresh catalyst) and that of Figure 4e (TEM image of spent catalyst) have been plotted (see Figures 4c and 4f, respectively). From TEM images (Figure 4a and 4e) and from the respective histograms, it was also noticed that the catalyst did

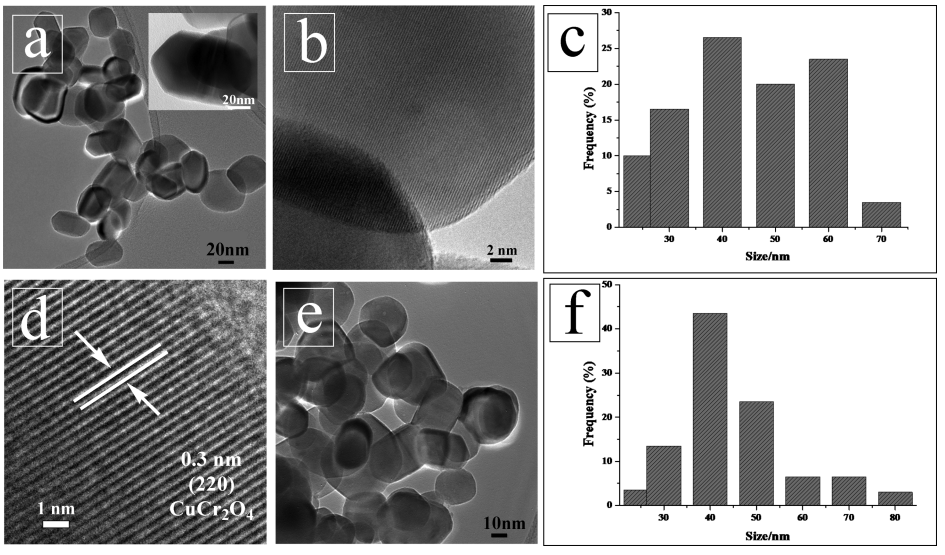

Figure 4. TEM images of the (a, b, d) fresh (at different resolutions) and (e) spent $CuCr_2O_4$ raspberry spinel particles. Panels c and f show their respective particle size distributions (histograms).

dx.doi.org/10.1021/am503722t | ACS Appl. Mater. Interfaces 2014, 6, 14451−14459

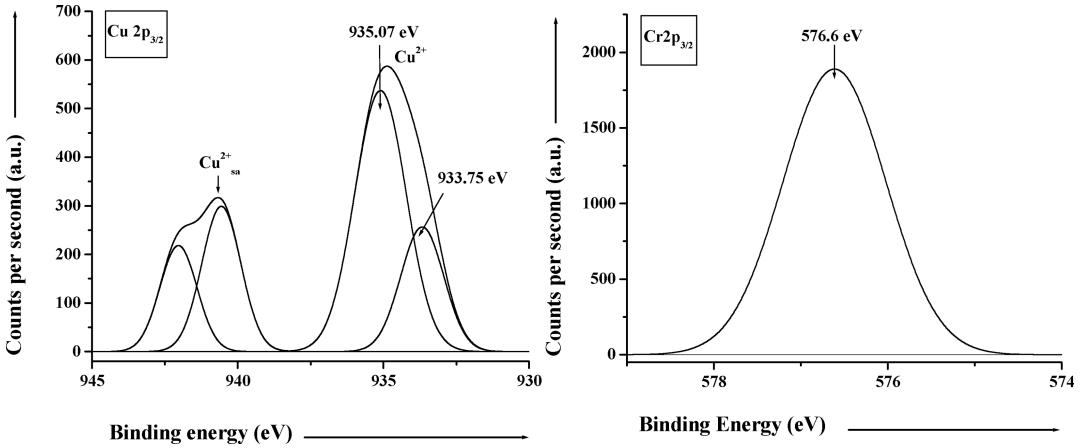

Figure 5. (Left) Cu $2p_{3/2}$ and (right) Cr $2p_{3/2}$ core level spectra (XPS) $CuCr_2O_4$ raspberry-spinel catalyst.

Scheme 1. Generation of the 3D-Raspberry-Like $CuCr_2O_4$ Spinel Catalyst

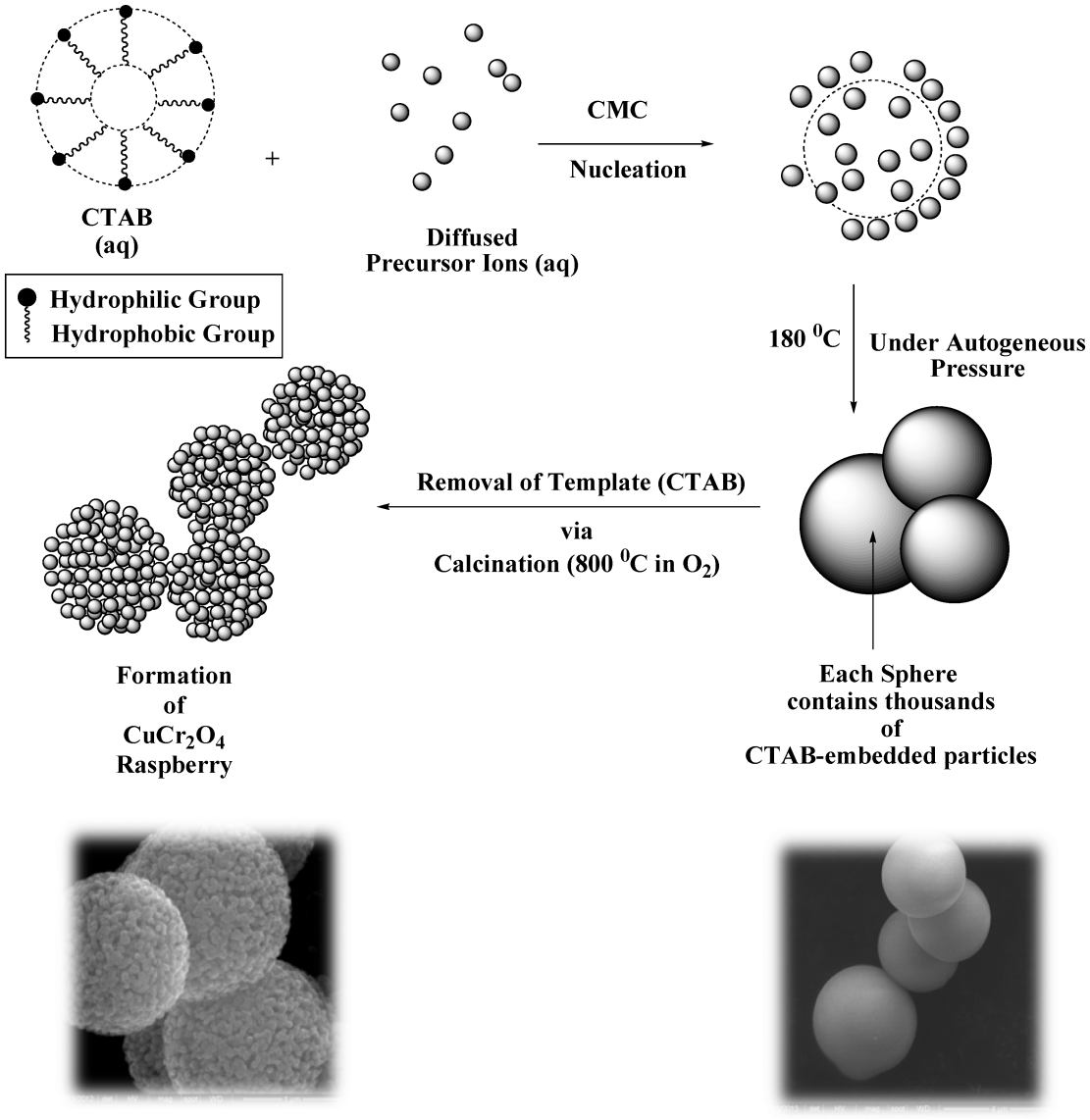

not undergo any significant change in during catalysis, even after 10 reuses.

The XPS spectra of Cu, Cr, and O in the $CuCr_2O_4$ spinel were presented in Figure 5 (left and right panels, respectively). Figure S4 in the Supporting Information, respectively. The Cu 2p spectrum of the fresh sample was characterized by two spin orbit doublets with strong satellite peaks. The Cu $2p_{3/2}$ signals fitted satisfactorily to two principal peak components at 935.0 and

dx.doi.org/10.1021/am503722t | ACS Appl. Mater. Interfaces 2014, 6, 14451−14459

933.7 eV. The binding energy (BE) for the Cu 2p peak was in close agreement with that of $CuCr_2O_4$. The low-energy component with Cu $2p_{3/2}$ is associated with Cu^{2+} in octahedral sites, whereas that the high energy component to Cu^{2+} in tetrahedral sites.[18,46]

Possible Formation Mechanism of the 3D Raspberry-Like Structure. The formation of 3D raspberry-like $CuCr_2O_4$ spinel particles can be explained on the basis of surfactant (CTAB) assisted nucleation−growth rate of the seed that actually determines the morphology of the final nanoparticle. As per the LaMer plot for the crystallization nucleation−growth process, the nucleation rate increases with decreasing surface energy.[47] In the presence of the surfactant, the surface tension of the solution is reduced, which lowers the energy needed to generate a new phase from the precursor ions.[48] The surfactant controls the nucleation rate by affecting the surface energy. According to Gibbs−Wulff theory, the equilibrium shape of a crystal is one that minimizes the surface energy for a given enclosed volume.[47] If the surface energy is isotropic, the equilibrium shape will be spherical, because the sphere has the minimum surface area. Before hydrothermal treatment, spherical nanoparticles of Cu−Cr are generated, since this represents the lowest possible surface energy. Hydrothermal treatment probably interferes with the surface energy to be and the particles aggregate into 3D nanostructures. In a control experiment, without the addition of surfactant CTAB, we failed to obtain the uniform 3D raspberry-like micro/nanocomposite structure (see Figure S5 in the Supporting Information), reflecting the structure-directing property of CTAB under hydrothermal conditions. Therefore, it can be suggested tentatively that CTAB molecules facilitate the assembly of almost-spherical nanoparticles into the 3D raspberry-like structure. Moreover, it also acted as a stabilizer to prevent nanoparticles from aggregation. The assembly effect of CTAB is assisted in basic pH,[49] and the role of CTAB in the generation of 3D raspberry-like $CuCr_2O_4$ spinel particles was furthermore confirmed when in a control experiment, when all the reagents were used without pH maintenance (pH ≪7), agglomerated particles with indefinite morphology were obtained (see Figure S5a in the Supporting Information). Hydrazine probably acted as a capping agent to control further growth of the particles; this is probably why we obtained particles with irregular and comparatively larger size in the absence of hydrazine, although a raspberry-like structure was noticed (see Figure S5c in the Supporting Information) Hydrothermal treatment, which is the genesis of autogenous pressure, is probably also responsible for the generation of 3D raspberry-like $CuCr_2O_4$ spinel particles. When we tried to synthesize 3D raspberry-like $CuCr_2O_4$ spinel particles without hydrothermal treatment, we obtained nanoparticles with irregular shapes and, more importantly, 3D architectures were not built (see Figure S6 in the Supporting Information). Although the mechanism for the formation of nanostructures is not very clear, we believe that CTAB, NH_4OH, hydrazine solutions, and the overall hydrothermal treatment each played an important role in orchestrating the 3D raspberry-like $CuCr_2O_4$ spinel particles. On the basis of the above discussion, the illustration for the possible formation mechanism of 3D raspberry-like $CuCr_2O_4$ spinel particles prepared in the presence of CTAB is shown in Scheme 1. In order to elucidate the growth process of 3D raspberry-like architectures, a series of time-dependent experiments were performed and we followed the growth steps of the samples at various reaction stages by SEM. It was also observed that a crystallization time of at least 18 h is necessary for the formation of a raspberry-like structure with almost-uniform sizes. Prolonged crystallization time (>18 h) resulted in the formation of polydispersed particles (Figure 6).

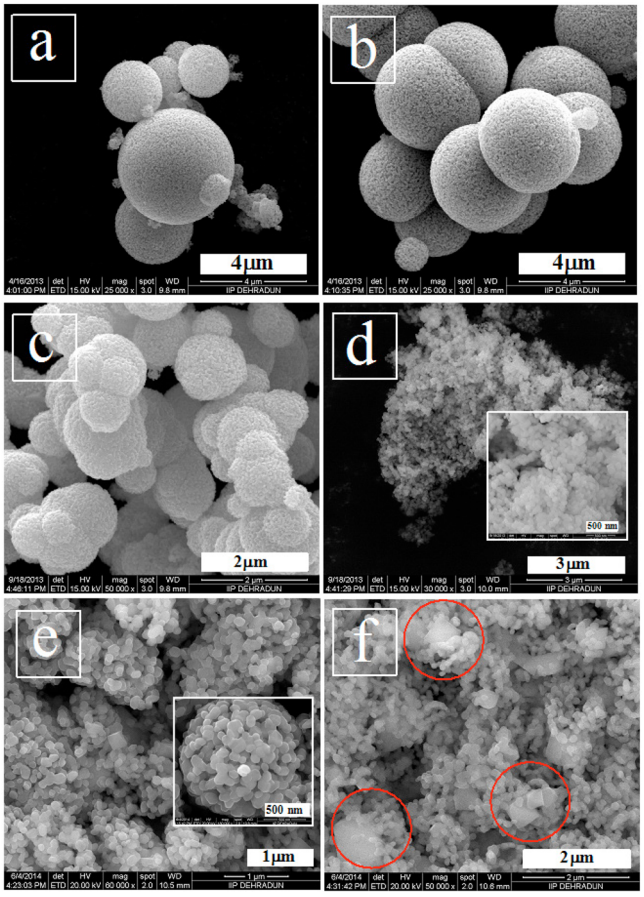

Figure 6. SEM micrographs of the Cu−Cr samples prepared by maintaining hydrothermal treatment (180 °C) for (a) 6 h, (b) 18 h, (c) 72 h, and (d) 7 days; SEM micrographs of the Cu-Cr samples prepared via hydrothermal treatment (e) after 7 days of continuous stirring and (f) after 7 days of aging, followed by hydrothermal treatment.

The driving force for the formation of raspberry morphology by means of interaction among the individual nanoparticles may be due to several factors, which include crystal-face attraction, electrostatic and dipolar fields associated with the aggregate, van der Waals forces, hydrophobic interactions, hydrogen bonds, etc. without any external intervention.[10] Moreover, the self-assemble- directing effect of the "soft template" CTAB and the contribution of the Ostwald ripening process cannot be avoided. It is worth mentioning that precursors of Cr^{6+} are necessary for the formation of the raspberry-like structure. This hypothesis was confirmed when other precursors of chromium were used, such as $CrCl_3$, $Cr(NO_3)_3{\cdot}9H_2O$, $KCr(SO_4)_2{\cdot}12(H_2O)$ (chrome alum), where chromium exists as chromium(III), a 3D raspberry-like morphology was not formed; however, a raspberry-like structure formation was noticed when $K_2Cr_2O_7$ was used as the chromium precursor (see Figure S7 in the Supporting Information). Moreover, when chromium(III) oxide was prepared by using $(NH_4)_2Cr_2O_7$, CTAB (basic medium), and hydrazine, a 3D-strawberry-like structure developed, which is entirely different from commercial chromium(III) oxide and even chromium(III) oxide obtained by heating $(NH_4)_2Cr_2O_7$ at 600 °C (see Figures S8 and S9 in the Supporting Information),

Table 2. Reaction Conditions of Catalytic Oxidation of Benzene[a]

			S_P(%)[d]					
entry	catalyst[b]	C_B (%)[c]	Φ_{OH}	catachol, Cat	hydroquinone, HQ	others	Y_P (%)[e]	$E°$ (%)[f]
1	CuO^{COM}	6.6	5.5	50	43	1.5	0.3	0.06
2	Cu_2O^{COM}	6.9	7.5	52.5	38	2.0	0.5	0.1
3	$Cr_2O_3{}^{COM}$	7.8	3.0	54	40	3.0	0.2	0.04
4	$CuCr_2O_4{}^{COM}$	17.5	15.5	46	36	2.5	2.7	0.54
5	$CuO-Cr_2O_3{}^{IMP}$	13.8	15.0	48	36	1.0	2.0	0.4
6	$CuO-Cr_2O_3{}^{CPM}$	13.5	15.8	44	38	2.2	2.1	0.42
7[g]	$CuO-Cr_2O_3$	37.5	68	17	13	2.0	25.5	5.1
8	CuO^{SRF}	7.0	6.5	47	44	2.5	0.4	0.08
9	$Cr_2O_3{}^{SRF}$	7.5	4.0	50	43	3.0	0.2	0.04
10[h]	$CuCr_2O_4{}^{RB}$	68.5	95	3	1.5	0.5	65.0	13.0
11[i]	$CuCr_2O_4{}^{RB}$	67.0	93	4	2	1.0	62.3	12.5
12[j]	$CuCr_2O_4{}^{RB}$	22.0	75.0	14	9	2.0	16.5	3.3
13[k]	$CuCr_2O_4{}^{RB}$	18.0	68.0	18	12	2.	12.2	2.4
14	no catalyst							

[a]Typical reaction conditions: solvent (acetonitrile) = 10 mL, substrate (benzene) = 1 g, catalyst= 0.08 g, benzene: H_2O_2 (molar ratio) = 1:5, reaction temperature = 80 °C; time = 10 h. [b]COM = commercial; IMP = impregnation method; CPM = coprecipitation method; SRF = surfactant-promoted; RB = raspberry-like. [c]C_B = conversion of benzene based upon the FID-GC using methanol as external standard = [moles of benzene reacted/initial moles of benzene used] × 100. [d]S_P = selectivity to phenol = [moles of products produced/mols of benzene reacted] × 100. [e]Y_P = yield of phenol = $C_B \times S_P/100$. [f]$E°$ = H_2O_2 efficiency = [moles of phenol formed/total moles of H_2O_2 added] × 100. [g]Copper nanoclusters supported on Cr_2O_3. [h]Prepared $CuCr_2O_4$ spinel nanoparticles. [i]Catalyst after 10 reuses. [j]Solvent = *n*-octane. [k]Solvent = DMF.

indicating the active participation of Cr^{6+} rather than Cr^{3+} in the self-assembly process during the micelle formation process.

Catalytic Oxidation Reaction. The reactions of the different Cu−Cr catalyst for selective oxidation of benzene to phenol are shown in Table 2. The prepared $CuCr_2O_4$ raspberry catalyst showed better catalytic activity than commercial catalysts and even better than Cu nanoclusters supported on Cr_2O_3 catalyst (see entries 1−7 in Table 2), which indicated the necessity of the spinel phase. Furthermore, the commercial $CuCr_2O_4$ spinel showed poor activity, compared to our so-prepared $CuCr_2O_4$ raspberry-like catalyst. This experimental finding can be attributed to the fact that the commercial $CuCr_2O_4$ spinel possesses particles that are of larger size, are not uniform (see Figure S10 in the Supporting Information), and have less BET surface area (5 m^2 g^{-1}). Therefore, the key sources for the higher activity of the $CuCr_2O_4$ raspberry-like catalyst, compared to the commercial spinel in the benzene hydroxylation reaction, is the presence of nanoparticles that have a high surface-to-volume ratio (BET surface area = 68 m^2 g^{-1}). Copper nanoclusters supported on a Cr_2O_3 catalyst showed activity in benzene hydroxylation; however, they suffered serious leaching. Moreover, we also prepared CuO (denoted as CuO^{SRF}) and Cr_2O_3 (denoted as $Cr_2O_3{}^{SRF}$) hydrothermally in the presence of CTAB and hydrazine (following the same preparation method as that of the $CuCr_2O_4$ raspberry-like catalyst) and conducted benzene hydroxylation reactions under the similar conditions (see entries 8 and 9 in Table 2). However, we still noticed that these materials were proven to be catalytically inactive in benzene hydroxylation.

Liquid-phase benzene hydroxylation reaction over the $CuCr_2O_4$ raspberry-like catalyst was speculated to be dependent on various reaction parameters, such as reaction temperature, concentration of oxidant, amount of catalyst, etc. We noticed that the benzene hydroxylation reaction was highly dependent on reaction temperature. At room temperature (35 °C), only 3.5% of benzene conversion was noticed. With increasing reaction temperature, the yield of the desired product (i.e., phenol) increased. The yield of phenol reached ∼10% at 50 °C and 65% at 80 °C over this catalyst (see Figure S11 in the Supporting Information). Further raising the temperature to 90 °C, there was no marked increase in the conversion of benzene, presumably because of the rapid decomposition of H_2O_2 at this temperature; but the selectivity to phenol (Φ_{OH}) decreased sharply to 88%, because of the formation of overoxidized products, namely catachol (Cat) and hydroquinone (HQ). We also studied the activity of the $CuCr_2O_4$ raspberry-like catalyst with different benzene:H_2O_2 molar ratios. When the benzene:-H_2O_2 molar ratio was 1:1 or 1:2.5, although the selectivity was >95%, the conversion of benzene was very low. This phenomenon can be attributed to the fact that the decomposition of H_2O_2 over $CuCr_2O_4$ surface was prominent.[50] When the benzene:H_2O_2 molar ratio was above 1:5, rapid decrement in total yield of phenol was observed, because of the formation of overoxidized product(s) (see Figure S12 in the Supporting Information). The benzene hydroxylation reaction also was dependent on the amount of catalyst used. Without any catalyst, the conversion of benzene was too poor to be detected (see entry 14 in Table 2), because of auto-oxidation of the benzene. With the increment of catalyst weight, an increment in phenol yield was noticed (see Figure S13 in the Supporting Information). Further increment of the catalyst led to a decrease in phenol selectivity, probably due to the increment in active sites of catalyst, which compelled the benzene molecules to overoxidize. Maintaining all the optimum conditions, when the reaction was allowed to run for hours, it was noticed that, initially, the conversion of benzene was low. Probably, much time was taken for the activation of the benzene ring; gradually grater conversion of benzene was speculated with time. We also observed that, with further increase in time, although there was higher conversion of benzene, but selectivity to phenol decreased sharply due to the inevitable oxidation of phenol to catechol (Cat) and hydroquinone (HQ), and polymerization of phenol (see Figure S14 in the Supporting Information).

Solvent (acetonitrile) played a very crucial role in the benzene hydroxylation reaction. When acetonitrile was employed as the solvent, the substrate benzene was miscible in acetonitrile, and

the catalyst could be well-dispersed. Dissociation of H_2O_2 over $CuCr_2O_4$ generates the active species $^{\bullet}OH$ (free hydroxy radical). During the benzene hydroxylation reaction, these hydroxy radicals behave as an electrophile in this reaction[51] and attack the activated C−H bond, which is adjacent to the π-system (phenyl ring), by means of homolytic C−H bond cleavage mechanism; thereby hydroxylated benzene (i.e., phenol molecules) are produced on the surface of the catalyst. This hydroxylation path is facilated by MeCN (solvent) molecules; consequently, high yield of phenol in acetonitrile was furnished. When *n*-octane and dimethylformamide (DMF) were used as solvents (entries 12 and 13 in Table 2), the catalyst showed very poor activity. Although high phenol selectivity was achieved in these solvents, but the conversion of benzene was very less. This can be attributed to the fact that *n*-octane is highly hydrophobic and DMF is highly hydrophilic in nature.[28] *n*-Octane and DMF quantitatively extract benzene and H_2O_2, as well as hydrated $^{\bullet}OH$ radicals, respectively, inhibiting a barrier between the catalyst surface, the reactant (benzene), and oxidant molecules, thereby waning the entire catalytic system.

Reusability Test. At the end of the reaction, the catalyst was filtered in the hot condition and was dried for 12 h at 100 °C. Recycling and reusability of the catalyst was examined by introducing the used catalyst subsequently 10 times to perform the catalytic oxidation. The reusability of the 3D $CuCr_2O_4$ catalyst was studied without regeneration of the catalyst in the same experimental condition. The catalyst showed 93% selectivity, even after 10 successive runs (see Figure S15 in the Supporting Information). The raspberry-like $CuCr_2O_4$ catalyst shows its high activity until 10 recycles. This may be attributed to the extreme stable spinel phase with a 3D structure, which inhibits the positions of the individual elements to be displaced. Interestingly, no leaching of Cr metal was detected, probably because of the extremely strong bindings of Cr atom in framework maintaining the 3D raspberry structure. The amount of Cu and Cr present in the spent catalyst (after 10 recycles) is almost same to that of the fresh catalyst (as estimated by ICP-AES; see Table 1), establishing that there was no leaching and the reaction was truly heterogeneous in nature. After the 11th run, a negligible amount of leaching of Cu as detected by ICP-AES (concentration of Cu was <2 ppb).

CONCLUSIONS

In summary, we have presented a facile, water-based, low-temperature synthesis of self-assembled $CuCr_2O_4$ spinel with a unique three-dimensional (3D) raspberry-like nanostructure. The initial investigation showed that it was a two-stage process, where nanoparticles were formed first, followed by organized assembly of these nanoparticles into raspberry-like microspheres. It was possible to tune the size of the microspheres by varying the preparation conditions. This synthesis could easily be scaled up, because of its simplicity. Moreover, the high thermal stability and reusability of the catalyst, and its excellent ability in the hydroxylation of benzene to phenol at liquid phase using H_2O_2 as the oxidant, may be a potential alternative path of the conventional cumene process.

ASSOCIATED CONTENT

Supporting Information

SEM images, XPS, TGA, effect of different reaction parameters on benzene hydroxylation, etc. This material is available free of charge via the Internet at http://pubs.acs.org.

AUTHOR INFORMATION

Corresponding Author

*Tel.: +91135 2525 917. Fax: +91 1352660202. E-mail: raja@iip.res.in.

Present Address

[†]Catalytic Conversion & Processes Division, CSIR-Indian Institute of Petroleum, Dehradun-248005, India.

Notes

The authors declare no competing financial interest.

ACKNOWLEDGMENTS

S.S.A. thanks CSIR and S.G. thank UGC, India for the fellowship. The Director, CSIR-IIP, is acknowledged for his help and encouragement. R.B. thanks CSIR, New Delhi, for financial support in the form of the 12 FYP Project (CSC-0125, CSC-0117). The authors thank Analytical Science Division, Indian Institute of Petroleum for analytical services.

ABBREVIATIONS

CTAB, cetyltrimethylammonium bromide; SEM, scanning electron microscopy; TEM, transmission electron microscopy; TGA, thermogravimetric analysis; XPS, X-ray photoelectron spectroscopy; XRD, X-ray diffraction

REFERENCES

(1) Park, S.; Lim, J. H.; Chung, S. W.; Mirkin, C. A. Self-assembly of Mesoscopic Metal-Polymer Amphiphiles. *Science* **2004**, *303*, 348−351.

(2) Mo, M.; Yu, J. C.; Zhang, L. Z.; Li, S. K. A. Self-Assembly of ZnO Nanorods and Nanosheets into Hollow Microhemispheres and Microspheres. *Adv. Mater.* **2005**, *17*, 756−760.

(3) Service, R. F. How far can we push Chemical Self-Assembly? *Science* **2005**, *309*, 95.

(4) Zhong, L. S.; Hu, J. S.; Liang, H. P.; Cao, A. M.; Song, W. G.; Wan, L. J. Self-Assembled 3D Flowerlike Iron Oxide Nanostructures and Their Application in Water Treatment. *Adv. Mater.* **2006**, *18*, 2426−2431.

(5) Ko, W. Y.; Chen, L. J.; Chen, Y. H.; Chen, W. H.; Lu, K. M.; Yang, J. R.; Yen, Y. C.; Lin, K. J. One-Step Solvothermal-Processed 3D Spinel-Type Manganese Oxide Microspheres and Their Improved Supercapacitive Properties. *J. Phys. Chem. C* **2013**, *117*, 16290−16296.

(6) Chen, L. Y.; Zhang, Z. D.; Wang, W. Z. Self-Assembled Porous 3D Flowerlike β-In_2S_3 Structures: Synthesis, Characterization, and Optical Properties. *J. Phys. Chem. C* **2008**, *112*, 4117−4123.

(7) Whitesides, G. M.; Boncheva, M. Perspective-Supramolecular Chemistry and Self-Assembly Special Feature. *Proc. Natl. Acad. Sci. U.S.A.* **2002**, *99*, 4769−4774.

(8) Stöber, W.; Fnk, A.; Bohn, E. J. Controlled Growth of Monodisperse Silica Spheres in the Micron Size Range. *J. Colloid Interface Sci.* **1968**, *26*, 62−69.

(9) Ahmed, A.; Ritchie, H.; Myers, P.; Zhang, H. One-Pot Synthesis of Spheres-on-Sphere Silica Particles from a Single Precursor for fast HPLC with Low Back Pressure. *Adv. Mater.* **2012**, *24*, 6042−6048.

(10) Ahmed, A.; Clowes, R.; Willneff, E.; Ritchie, H.; Myers, P.; Zhang, H. Silica of Uniform Porous Silica Microspheres with Hydrophilic Polymer as Stabilizing Agent. *Ind. Eng. Chem. Res.* **2010**, *49*, 602−608.

(11) Li, Z.; Ravaine, V.; Ravaine, S.; Garrigue, P.; Kuhn, A. Raspberry-like Gold Microspheres: Preparation and Electrochemical Characterization. *Adv. Funct. Mater.* **2007**, *17*, 618−622.

(12) Zhu, L. P.; Zhang, W. D.; Xiao, H. M.; Yang, Y.; Fu, S. Y. Facile Synthesis of Metallic Co Hierarchical Nanostructured Microspheres by a Simple Solvothermal Process. *J. Phys. Chem. C* **2008**, *112*, 10073−10078.

(13) Wang, C.; Yan, J.; Cui, X.; Wang, H. Synthesis of Raspberry-like Monodisperse Magnetic Hollow Hybrid Nanospheres by Coating

Polystyrene Template with Fe_3O_4@SiO_2 Particles. *J. Colloid Interface Sci.* **2011**, *354*, 94−99.
(14) Xu, X. W.; Zhang, X. M.; Liu, C.; Yang, Y. L.; Liu, J. W.; Cong, H. P.; Dong, C. H.; Ren, X. F.; Yu, S. H. One-Pot Colloidal Chemistry Route to Homogeneous and Doped Colloidosomes. *J. Am. Chem. Soc.* **2013**, *135*, 12928−12931.
(15) Adkins, H.; Connor, R. The Catalytic Hydrogenation of Organic Compounds over Copper Chromite. *J. Am. Chem. Soc.* **1931**, *53*, 1091−1095.
(16) Roy, S.; Ghose, J. Synthesis and Studies on Some Copper Chromite Spinel Oxide Composites. *Mater. Res. Bull.* **1999**, *34*, 1179−1186.
(17) Stroupe, J. D. An X-ray Diffraction Study of the Copper Chromites and of the Copper−Chromium Oxide Catalyst. *J. Am. Chem. Soc.* **1949**, *71*, 569−572.
(18) Severino, F.; Brito, J. L.; Laine, J.; Fierro, L. G.; Agudoy, A. L. Nature of Copper Active Sites in the Carbon Monoxide Oxidation on $CuAl_2O_4$ and $CuCr_2O_4$ Spinel Type Catalysts. *J. Catal.* **1998**, *177*, 82−95.
(19) Kawamoto, A. M.; Pardini, L. C.; Rezende, L. C. Synthesis of Copper Chromite Catalyst. *Aerosp. Sci. Technol.* **2004**, *8*, 591−598.
(20) Jacobs, P. W. M.; Whitehead, H. M. Decomposition and Combustion of Ammonium Perchlorate. *Chem. Rev.* **1969**, *69*, 551−590.
(21) Armstrong, R. W.; Baschung, B.; Booth, D. W. Enhanced Propellant Combustion with Nanoparticles. *Nano Lett.* **2003**, *3*, 253−255.
(22) Rajeev, R.; Devi, K. A.; Abraham, A.; Krishnan, K.; Krishnan, T. E.; Ninan, K. N.; Nair, C. G. R. Thermal Decomposition Studies (Part 19): Kinetics and Mechanism of Thermal Decomposition of Copper Ammonium Chromate Precursor to Copper Chromite Catalyst and Correlation of Surface Parameters of the Catalyst with Propellant Burning Rate. *Thermochim. Acta* **1995**, *254*, 235−247.
(23) Valdés-Solís, T.; Marbán, G.; Futertes, A. B. Preparation of Nanosized Perovskites and Spinels Through a Silica Xerogel Template Route. *Chem. Mater.* **2005**, *17*, 1919−1922.
(24) Tanaka, Y.; Takeguchi, T.; Kikuchi, R.; Eguchi, K. Influence of Preparation Method and Additive for Cu−Mn Spinel Oxide Catalyst on Water Gas Shift Reaction of Reformed Fuels. *Appl. Catal., A* **2005**, *279*, 59−66.
(25) Centi, G.; Perathoner, S. One-Step H_2O_2 and Phenol Syntheses: Examples of Challenges for New Sustainable Selective Oxidation Processes. *Catal. Today* **2009**, *143*, 145−150.
(26) Tada, M.; Bal, R.; Sasaki, T.; Uemura, Y.; Inada, Y.; Tanaka, S.; Nomura, M.; Iwasawa, Y. Novel Re-Cluster/HZSM-5 Catalyst for Highly Selective Phenol Synthesis from Benzene and O_2: Performance and Reaction Mechanism. *J. Phys. Chem. C* **2007**, *111*, 10095−10104.
(27) Xin, H.; Koekkoek, A.; Yang, Q.; van Santen, R. A.; Li, C.; Hensen, E. J. M. A Hierarchical Fe/ZSM-5 Zeolite with Superior Catalytic Performance for Benzene Hydroxylation to Phenol. *Chem. Commun.* **2009**, 7590−7592.
(28) Bianchi, D.; Bortolo, R.; Tassinari, R.; Ricci, M.; Vignola, R. A Novel Iron-Based Catalyst for the Biphasic Oxidation of Benzene to Phenol with Hydrogen Peroxide. *Angew. Chem.* **2000**, *39*, 4321−4323.
(29) Balducci, L.; Bianchi, D.; Bortolo, R.; D'Aloisio, R.; Ricci, M.; Tassinari, R.; Ungarelli, R. Direct Oxidation of Benzene to Phenol with Hydrogen Peroxide over a Modified Titanium Silicalite. *Angew. Chem.* **2003**, *115*, 5087−5090.
(30) Chen, J.; Gaoa, S.; Xu, J. Direct Hydroxylation of Benzene to Phenol over a New Vanadium-Substituted Phosphomolybdate as a Solid Catalyst. *Catal. Commun.* **2008**, *9*, 728−733.
(31) Bal, R.; Tada, M.; Sasaki, T.; Iwasawa, Y. Direct Phenol Synthesis by Selective Oxidation of Benzene with Molecular Oxygen on an Interstitial-N/Re Cluster/Zeolite Catalyst. *Angew. Chem.* **2006**, *45*, 448−452.
(32) Tani, M.; Sakamoto, T.; Mita, S.; Sakaguchi, S.; Ishii, Y. Hydroxylation of Benzene to Phenol under Air and Carbon Monoxide catalyzed by Molybdovanadophosphoric acid. *Angew. Chem.* **2005**, *44*, 2586−2588.
(33) Panov, G. I.; Kharitonov, A. S.; Sobolev, V. I. Oxidative Hydroxylation using Dinitrogen Monoxide: A Possible Route for Organic Synthesis over Zeolites. *Appl. Catal., A* **1993**, *98*, 1−20.
(34) Smith, J. R. L.; Norman, R. O. C. 539. Hydroxylation. Part I. The Oxidation of Benzene and Toluene by Fenton's reagent. *J. Chem. Soc.* **1963**, 2897−2905.
(35) Piera, J.; Backvall, J. E. Catalytic Oxidation of Organic Substrates by Molecular Oxygen and Hydrogen Peroxide by Multistep Electron Transfer—A Biomimetic Approach. *Angew. Chem.* **2008**, *47*, 3506−3523.
(36) Tanev, P. T.; Chibwe, M.; Pinnavaia, T. J. Titanium-Containing Mesoporous Molecular Sieves for Catalytic Oxidation of Aromatic Compounds. *Nature* **1994**, *368*, 321−323.
(37) Zhang, F.; Guo, M.; Ge, H.; Wang, J. Hydroxylation of Benzene with Hydrogen Peroxide over Highly Efficient Molybdovanadophosphoric Heteropoly Acid Catalysts. *Chin. J. Chem. Eng.* **2007**, *15*, 895−898.
(38) Borah, P.; Ma, X.; Nguyen, K. T.; Zhao, Y. A Vanadyl Complex Grafted to Periodic Mesoporous Organosilica: A Green Catalyst for Selective Hydroxylation of Benzene to Phenol. *Angew. Chem.* **2012**, *51*, 7756−7761.
(39) Zhao, P.; Leng, Y.; Wang, J. Heteropolyanion-paired Cross-Linked Ionic Copolymer: An Efficient Heterogeneous Catalyst for Hydroxylation of Benzene with Hydrogen Peroxide. *Chem. Eng. J.* **2012**, *204*, 72−78.
(40) Zhao, P.; Wang, J.; Chen, G.; Zhou, Y.; Huang, J. Phase-Transfer Hydroxylation of Benzene with H_2O_2 Catalyzed by a Nitrile-Functionalized Pyridinium Phosphovanadomolybdate. *Catal. Sci. Technol.* **2013**, *3*, 1394−1404.
(41) Long, Z.; Zhou, Y.; Chen, G.; Ge, W.; Wang, J. C_3N_4−$H_5PMo_{10}V_2O_{40}$: A Dual-Catalysis System for Reductant-Free Aerobic Oxidation of Benzene to Phenol. *Sci. Rep.* **2014**, *4*, 3651 DOI: 10.1038/srep03651.
(42) Acharyya, S. S.; Ghosh, S.; Adak, S.; Sasaki, T.; Bal, R. Facile Synthesis of $CuCr_2O_4$ Spinel Nanoparticles: A Recyclable Heterogeneous Catalyst for One Pot Hydroxylation of Benzene. *Catal. Sci. Technol.* **2014**, DOI: 10.1039/C4CY00615A.
(43) Acharyya, S. S.; Ghosh, S.; Bal, R. Catalytic Oxidation of Aniline to Azoxybenzene over $CuCr_2O_4$ Spinel Nanoparticle Catalyst. *ACS Sustainable Chem. Eng.* **2014**, *2*, 584−589.
(44) Cheng, W.; Dong, S.; Wang, E. Synthesis and Self-Assembly of Cetyltrimethylammonium Bromide-Capped Gold Nanoparticles. *Langmuir* **2003**, *19*, 9434−9439.
(45) Bajaj, R.; Sharma, M.; Bahadur, D. Visible Light-Driven Novel Nanocomposite ($BiVO_4$/$CuCr_2O_4$) for Efficient Degradation of Organic Dye. *Dalton Trans.* **2013**, *42*, 6736−6744.
(46) Pantaleo, G.; Liotta, L. F.; Venezia, A. M.; Deganello, G.; Ezzo, E. M.; El Kherbawi, M.; Atia, H. Support Effect on the Structure and CO Oxidation Activity of Cu-Cr Mixed Oxides over Al_2O_3 and SiO_2. *Mater. Chem. Phys.* **2009**, *114*, 604−611.
(47) Jiang, Z.; Xie, J.; Jiang, D.; Wei, X.; Chen, M. Modifiers-Assisted Formation of Nickel Nanoparticles and Their Catalytic Application to *p*-Nitrophenol Reduction. *CrystEngComm* **2013**, *15*, 560−569.
(48) Sun, X. M.; Chen, X.; Deng, Z. X.; Li, Y. D. A CTAB-Assisted Hydrothermal Orientation Growth of ZnO nanorods. *Mater. Chem. Phys.* **2002**, *78*, 99−104.
(49) Hashempour, M.; Razavizadeh, H.; Rezaie, H.; Hashempour, M.; Ardestani, M. Chemical Mechanism of Precipitate Formation and pH Effect on the Morphology and Thermochemical Co-Precipitation of W−Cu Nanocomposite Powders. *Mater. Chem. Phys.* **2010**, *123*, 83−90.
(50) Kazarnovsky, I. A. *Dokl. Akad. Nauk SSSR* **1975**, *221* (2), 353−356 (in Russ.).
(51) Dubey, A.; Rives, V.; Kannan, S. Catalytic Hydroxylation of Phenol over Ternary Hydrotalcites Containing Cu, Ni and Al. *J. Mol. Catal. A: Chem.* **2002**, *181*, 151−160.